A DNA nanoassembly-based approach to map membrane protein nanoenvironments

Elena Ambrosetti[1], Giulio Bernardinelli[1], Ian Hoffecker[1], Leonard Hartmanis[2], Georges Kiriako[1], Ario de Marco[3], Rickard Sandberg[2], Björn Högberg[1] & Ana I. Teixeira[1,*]

[1]Department of Medical Biochemistry and Biophysics, Karolinska Institutet, Sweden
[2]Department of Cell and Molecular Biology, Karolinska Institutet, Sweden
[3]Laboratory for Environmental and Life Sciences, University of Nova Gorica, Slovenia
[*]Corresponding Author: Ana I. Teixeira, ana.teixeira@ki.se

Abstract

Most proteins at the plasma membrane are not uniformly distributed but localize to dynamic domains of nanoscale dimensions. To investigate their functional relevance, there is a need for methods that enable comprehensive analysis of the compositions and spatial organizations of membrane protein nanodomains in cell populations. Here we describe the development of a non-microscopy based method for ensemble analysis of membrane protein nanodomains. The method, termed NANOscale DEciphEring of membrane Protein nanodomains (NanoDeep), is based on the use of DNA nanoassemblies to translate membrane protein organization information into a DNA sequencing readout. Using NanoDeep, we characterised the nanoenvironments of Her2, a membrane receptor of critical relevance in cancer. Importantly, we were able to modulate by design the inventory of proteins analysed by NanoDeep. NanoDeep has the potential to provide new insights into the roles of the composition and spatial organization of protein nanoenvironments in the regulation of membrane protein function.

Cells sense extracellular signals, such as protein ligands, through specialised proteins present on the cell surface called membrane receptors. The protein nanoenvironment, i.e. the composition and spatial organization of proteins surrounding membrane receptors, is dynamic and often modulated by ligand binding, suggesting that it has functional relevance[1-5]. Super-resolution microscopy has enabled the characterisation of the nanoscale spatial distributions of proteins at the cell membrane[6, 7]. Super-resolution imaging methods use detection of light emitted by fluorophores as a readout, which poses limitations on the number of proteins that can be analysed simultaneously. However, several recent developments such as PAINT[8, 9] and maS^{3}TORM[10] enable increased multiplexing in super-resolution imaging by stochastic binding of fluorescently labelled DNA oligos or by serial imaging, respectively. Automation strategies have improved considerably sampling fractions in super-resolution imaging[10, 11], but it is typically only feasible to image a small fraction of all protein nanodomains present in a cell population. DNA detection as a proxy for protein detection through the use of oligo-conjugated affinity binders has been used extensively for signal amplification[12] and analysis of proximity between pairs of proteins[13, 14]. Further, DNA sequencing is used as a readout in DNA microscopy, a new method to visualize the spatial organization of RNA and DNA molecules inside cells[15-17]. Here we present NanoDeep, a method that uses DNA sequencing to decipher the nanoscale spatial distribution of membrane proteins. This method allows for the detection *en masse* of the inventory of proteins that forms the nanoenvironment of any reference membrane protein in cell populations.

We demonstrate the application of NanoDeep to the analysis of protein nanoenvironments surrounding Human Epidermal Growth Factor Receptor 2 (Her2). Her2 cooperates with members of the Epithelial Growth Factor Receptor (EGFR) family of proteins (EGFR, Her2, Her3 and Her4) to regulate cell proliferation and differentiation during normal embryonic development[18]. Her2 is overexpressed in several cancers and its expression levels correlate with poor prognosis[18, 19]. Interestingly, the oncogenic capacity of Her2 is closely connected to the impact of overexpression on the frequency distributions of interactions between Her2 and EGFR family members at the cell membrane[20-22]. For example, Her2 overexpression leads to increased levels of Her2 and Her3 heterodimers, which drive more potent oncogenic signalling activity than the corresponding homodimers[19, 23-25]. Further, Her2-EGFR dimerization, driven by overexpression of one or both proteins, has been shown to lead to a more aggressive breast cancer phenotype[26]. Notably, new evidence supports the hypothesis that not only the formation of dimers but also of higher-order receptor

assemblies at cell membrane regulates Her2 function[27-31]. Although there are well established correlations between the levels of Her2 homo- and heterodimers and cancer aggressiveness, the roles of the composition of Her2 protein nanoenvironments for downstream signalling are poorly understood[25]. Using NanoDeep, we characterised the protein nanoenvironments of Her2 in model surfaces and in cells. We found that SKBR3 breast cancer cells that overexpress Her2 showed similar levels of occupancy of Her2, Her3 and EGFR in Her2 nanoenvironments compared to MCF7 breast cancer cells, which present basal levels of Her2. However, the higher expression levels of Her2 in SKBR3 cells correlated with higher total levels of Her2, Her3 and EGFR in Her2 nanoenvironments, compared to MCF7 cells. Further, stimulation of SKBR3 cells with the Her3 ligand Heregulin-β1 (HRG-β1) led to an increase in occupancy of Her2 and Her3, and to a lesser extent of EGFR, in Her2 nanoevinronments. Together, these results indicate that NanoDeep is able to characterize differences in protein nanoenvironments in different cellular contexts.

NanoDeep The NanoDeep method converts protein spatial distribution information into a DNA sequencing readout (Fig. 1). We designed a DNA nanoassembly, which we named NanoComb, composed of four single-stranded DNA (ssDNA) oligos, called prongs, that protrude from a double-stranded backbone at regular intervals. The prongs contain a barcode that identifies their position within the NanoComb. The first prong is defined as the reference prong and the remaining prongs are the detection prongs. The reference prong is preloaded with a binder that recognizes a reference protein, which is Her2 in our model workflow. This is done by conjugating the binder for the reference protein with an oligo that partially hybridizes with the reference prong (Fig. 1a). After incubating the NanoComb bearing the binder for the reference protein with fixed cells, a library of binders for the inventory of proteins to be analysed is added, each conjugated to an oligo containing a barcode that identifies the protein recognised by the binder (Fig. 1b). The oligos further contain a sequence, which is common to all binder-oligo conjugates, that is partially complementary to the detection prongs. Importantly, to prevent binder-oligo conjugates that are not bound to membrane proteins from hybridizing with the detection prongs, hybridization is blocked when conjugates are added to the cells and unblocked after washing away conjugates that are not bound to their target membrane proteins (Fig. 1c). The hybridization between the prongs and the binder oligos creates free 3' ends that act as primers for DNA polymerase (Fig. 1d), leading to the formation of double-stranded DNA (dsDNA) sequences that contain both the barcode for the position of the prong as well as the binder barcode (Fig. 1e). As specific nuclease sequences are incorporated in both the prongs and binder oligos, these dsDNA sequences can be cleaved by a nuclease (Fig. 1f) and analysed by next generation sequencing (NGS) (Fig. 1g), providing information on the composition and spatial organization of the nanoenvironment surrounding the reference protein across the cell population.
Super-resolution microscopy studies determined that the spacing of proteins in Her2 dimers is on average in the range of 10-20 nm[21, 29, 32] and that Her2 clusters in breast carcinoma cell lines have a mean diameter of 67 nm[27]. The detection prongs of the NanoCombs are positioned by design at 7, 14 and 21 nm relative to the reference prong, in an extended DNA conformation. As the NanoComb dimensions are below the persistence length of dsDNA, which is estimated to be around 50 nm[33], it has limited molecular flexibility and can be considered as having linear conformation on average. Therefore, the geometry of NanoCombs enables probing of the relevant length scale for the analysis of Her2 nanoenvironments.

Characterisation of NanoCombs and binder-oligo conjugates NanoCombs were produced by hybridizing a 100-nucleotide (nt) long ssDNA oligo (backbone) to four shorter oligos (prongs) partially complementary to the backbone (Fig. 2a,b). The prongs form a pattern of four ssDNA oligos with a period of 21 base pairs (bp), protruding from the same side of the backbone. The period of the prongs corresponds to a distance of 7 nm in an extended DNA conformation. The length of the protruding portion of the prongs is 36 and 31 bp for reference prong and detection prongs, respectively, corresponding to a maximum length of 12.5 nm, when double-stranded (Fig. 2a,b).
After folding the NanoCombs, we removed the excess prongs by using streptavidin-coated magnetic beads and taking advantage of the lower affinity of desthiobiotin compared to biotin (Supplementary Fig. 1). We monitored the assembly of NanoCombs with Surface Plasmon Resonance (SPR) assay, showing sequential hybridization of the four prongs with the backbone (Fig. 2c). We further confirmed NanoComb assembly and purification with native polyacrylamide gel electrophoresis (PAGE), which showed that the four prongs

hybridised with the backbone (Fig. 2d) and that the NanoCombs were purified from excess prongs (Supplementary Fig. 1).
We selected affibodies as binders due to their high affinity and small dimensions, minimizing the impact of the size of the binder *per se* on the spatial resolution of the method. To enable site specific conjugation with a stoichiometry of 1:1, we used a conjugation approach based on a self-labelling tag derived from a truncated VirD2 protein of *Agrobacterium tumefaciens*[34]. We produced fusion proteins between VirD2 and affibodies that bind the extracellular domains of three members of the EGFR family (EGFR, Her2 and Her3). SPR assay showed that all affibodies fused to VirD2 exhibited high affinity and selectivity for their specific targets (Extended Data Fig. 1). Further, native PAGE demonstrated efficient conjugation of the affibodies with the oligos (Extended Data Fig. 2a). We observed that the oligo conjugation caused a slight increase in the K_D of the affibodies that nevertheless did not prevent them from recognizing their targets with high affinity since the K_D was still in the nanomolar range, and, more significantly, the low dissociation rate (k_{off}) was preserved (Extended Data Fig. 2b).
To assess the hybridization of the affibody-oligo conjugates to the NanoCombs, we used direct (Fig. 2e) and reverse (Fig. 2f) SPR assays using anti-Her2 affibody-oligo conjugates as a test sample, which supported the specificity of the interaction between the NanoCombs and the affibody-oligo conjugates.

Toehold exchange strategy for specific binder detection In the model workflow presented here, the targeting step in NanoDeep consists of binding NanoCombs preloaded with anti-Her2 affibody (Her2-NanoCombs) to Her2. The detection step involves binding of anti-Her2, -Her3 and -EGFR affibody-oligo conjugates (binder library) to their targets and hybridization of the oligos to the detection prongs of the NanoCombs. Therefore, it is crucial that the hybridization of the binder library to the detection prongs of the NanoCombs occurs only when the affibodies are first bound to their target proteins. To address this, we developed a strategy based on toehold-mediated strand displacement[35, 36], widely used in dynamic DNA nanotechnology. To validate this strategy, biotinylated versions of the binder oligos were anchored to streptavidin coated SPR surfaces (Extended Data Fig.3). Hybridization to a blocking strand caused an increase in the SPR signal, which was followed by a decrease in the signal due to displacement of the blocking strand through strand migration upon adding an invading strand. The resulting unblocked oligos were able to hybridize to the NanoCombs, which led to an increase in the SPR signal (Extended Data Fig.3a). In the absence of strand invasion, the blocked oligos were not able to bind to the NanoCombs (Extended Data Fig.3b). To verify that the affibody-oligo conjugates were able to hybridize, following toehold exchange, to the detection prongs of Her2-NanoCombs, we performed SPR assays using surfaces that presented both ECD-Her2 and ECD-Her3. Her2-NanoCombs were incubated with the functionalised SPR surfaces (Fig. 3). Following washing, anti-Her3 affibody-oligo conjugates that were pre-hybridised to blocking strands were injected. After allowing for binding of the conjugates to ECD-Her3 on the SPR surfaces and washing away unbound conjugates, the blocking strand was displaced by adding the invading strand. To confirm that the detection prongs of the NanoCombs were able to bind to the unblocked anti-Her3 affibody-oligo conjugates, we introduced a second toehold-mediated exchange system that displaced the hybridization between the reference prong and the anti-Her2 affibody-oligo conjugate. In this manner, the NanoCombs were able to stay bound to the surface only if the anti-Her3 affibody-oligo conjugates were properly unblocked and were able to hybridize to the detection prongs. Accordingly, we did not observe significant loss of the SPR signal upon injection of the invading strand for the anti-Her2 affibody-oligo conjugate on samples where we performed unblocking of the anti-Her3 affibody-oligo conjugates (Fig. 3a-left). In contrast, the SPR signal decreased on surfaces that had not been treated with anti-Her3 conjugates (Fig. 3a-right). Using Electrophoretic Mobility Shift assay (EMSA), we further confirmed reversible blocking of the affibody-oligo conjugates, when performing the reactions in solution (Fig. 3b). Together, these results show that toehold-mediated strand displacement reversibly blocked the hybridization of affibody-oligo conjugates to the detection prongs of the NanoCombs with high efficiency.

Validation of enzymatic reactions to generate dsDNA sequences Once correct binding is established between the prongs of the NanoCombs and the binder oligos, two enzymatic reactions, DNA polymerization and cleavage, are needed to obtain the final dsDNA sequences that hold both the position and identity barcodes. Using SPR, we were able to monitor the release of NanoCombs and barcoded dsDNA fragments

from the surface, following successful T4 polymerase elongation and BamHI/EcoRI cleavage reactions (Fig. 4a,b). We further confirmed with native PAGE that we obtained the final barcoded fragments only from samples where both enzymatic reactions had occurred (Fig. 4c).

NGS decoding of barcoded dsDNA sequences We performed NanoDeep on model SPR surfaces, in which we were able to tune the composition and the surface density of bound proteins. We produced SPR surfaces that presented ECD-Her2 and ECD-Her3 at two different surface densities (Fig. 5a-left). We treated the surfaces with Her2-NanoCombs and performed NanoDeep using binder libraries consisting of anti-Her2 and anti-Her3 conjugates. To investigate whether the NGS analysis reflected the density of the proteins present on the surface, we correlated the SPR binding signal of the library (Fig. 5a-center) with the NGS reads originating from the detection prongs (detection sequences), scaled to the reads from the reference prongs (reference sequences). We observed that there was a correspondence between the SPR signal and the number of reads from the detection prongs (Fig. 5a-right). Next, we created surfaces presenting different combinations of the ECD-Her2, -Her3 and -EGFR (Fig. 5b-left) and performed NanoDeep using Her2-NanoCombs and binder libraries consisting of anti-Her2, -Her3 and -EGFR conjugates. SPR analysis showed that the binding of each of the library binders was specific to their respective targets (Extended Data Fig.4). NGS analysis of the resulting barcoded dsDNA fragments showed that the detection prongs were able to selectively detect the proteins present in each surface. Importantly, the distribution of reads for position barcodes indicated unbiased probing by the detection prongs of the NanoComb.

Next, we performed NanoDeep on Her2-expressing cancer cells. We confirmed that NanoDeep only generated reference and detection sequences when Her2-NanoCombs were pre-loaded with anti-Her2 affibodies (Extended Data Fig.5). To verify the correlation between NGS reads from reference sequences and the amount of Her2-NanoCombs that were bound to the cells, we treated SKBR3 cells with increasing concentrations of Her2-NanoCombs. We found that there was a linear correlation between the levels of reference sequences and the concentration of NanoCombs. In subsequent experiments, NGS reads from reference sequences were used to scale the reads from detection sequences (Fig. 6a). Further, we used a concentration of NanoCombs of 5 μg/mL, which is in the lower region of the curve, to allow detection of the reference protein in its nanoenvironment and to avoid molecular crowding effects that could impair binding of the binder library.
We used NanoDeep to analyse Her2 nanoenvironments in SKBR3 and MCF7 breast cancer cells, which exhibit high and low expression levels of Her2, respectively. The rationale for testing cell lines with different expression levels is that the oncogenic capacity of Her2 is associated with the effects of overexpression on the frequency distributions of interactions between Her2 and other EGFR family members at the cell membrane[19-22]. NGS analysis of reference sequences demonstrated that the NanoDeep approach detected the differences in Her2 expression levels between the two cell lines. Analysis of the detection sequences provided information on the Her2 nanoenvironments. As shown in the heatmaps, the occupancies of Her2, Her3 and EGFR were similar in the two cell lines (Fig. 6b). However, the total levels of Her2, Her3 and EGFR were higher in SKBR3 cells compared to MCF7 cells, supporting the notion that overexpression of Her2 leads to a higher number of interactions between Her2 and other EGF receptors. These results are consistent with previous reports showing that heterodimers between Her2 and other EGFR family members can form in Her2-expressing cancer cells, irrespective of Her2 expression levels[22, 25]. As a control, we performed NanoDeep on SKBR3 cells using Her3-NanoCombs and the binder library targeting Her2, Her3 and EGFR (Extended Data Fig.6). The number of NGS reads originating from the reference sequence of Her3-NanoCombs were lower than those from Her2-NanoCombs, consistent with the lower levels of expression of Her3 compared to Her2 in SKBR3 cells. The occupancies of Her2, Her3 and EGFR in the Her3 nanoenvironment differed from those obtained with Her2-NanoCombs. In particular, the levels of Her2 were higher than the levels of Her3 in the Her3 nanoenvironment and vice versa for the Her2 nanoenvironment (Fig. 6b). As a negative control, we used SH-SY5Y cells, which show minimal levels of expression of Her2. Accordingly, NGS analysis did not identify any reference or detection sequences (Extended Data Fig.7).

To investigate whether NanoDeep can detect differences in cellular states due to ligand binding to membrane receptors, we treated SKBR3 cells with HRG-β1, one of the isoforms of Heregulin growth factor. HRG-β1 binds to Her3, inducing heterodimerization with Her2[37, 38] and, to a lesser extent with EGFR[32], leading to increased cell proliferation in breast cancer cell lines[22, 37, 39, 40]. NanoDeep revealed that treatment of SKBR3 cells with HRG-β1 led to increased occupancy of Her2 and Her3, and to a lesser extent EGFR, in the nanoenvironment of Her2 (Fig. 6c). The observed increase of Her3 in the nanoenvironment of Her2 is in line with the known mechanism by which HRG-β1 triggers the interaction between Her2 and Her3[38]. Further, the presence of increased levels of Her2 indicates that HRG-β1 binding to Her3 promotes membrane interaction networks that are more complex than pairwise interactions. A molecular basis for the specific functions of higher-order structures has been described for EGFR, where self-association of ligand bound dimers leads to cooperativity in the activation of kinase domains[29, 41]. However, the composition and roles of higher-order structures in EGFR family mediated signalling are still poorly characterised.

To extend the characterisation of Her2 nanoenvironments beyond EGFR family members, we expanded the binder library to include binders targeting integrin α5β1 and CD63, which are membrane proteins that have been reported to interact with Her2. Additionally, we included an aptamer targeting the transferrin receptor, CD71, which is expressed in SKBR3 cells and is unrelated to Her2 signalling. Integrin α5β1 is involved in tumour progression[42-44] and both integrin α5 and integrin β1 have been shown to interact directly with Her2[45, 46]. CD63 is involved in regulation of endocytosis[47-49] and bispecific antibodies targeting Her2 and CD63 were reported to promote Her2 endocytosis[50]. To target integrin α5β1, we used the small peptide ATN-161[43-45, 51], which we conjugated to a DNA oligo using amine coupling (Extended Data Fig.8). We exploited the SpyCatcher-SpyTag system to covalently bind an anti-CD63 nanobody fused to SpyTag (see Methods) to SpyCatcher conjugated to a DNA oligo (Extended Data Fig.9). Further, we modified an aptamer specific for CD71[52, 53] by extending the aptamer sequence to include a barcoded oligo (Extended Data Fig.10).
We performed NanoDeep on SKBR3 cells using Her2-NanoCombs and a binder library that included binders targeting Her2, Her3, EGFR, CD63, integrin α5β1 and CD71 (Fig. 7). We found that the occupancies of Her2, Her3 and EGFR were comparable to those obtained when probing only EGFR family members. Further, we detected the presence of both CD63 and integrin α5β1 but not CD71 in the Her2 nanoenvironment. Conversely, when we performed NanoDeep using CD71-NanoCombs, we were able to target CD71 but did not detect Her2, Her3 and EGFR in the nanoenvironment of CD71. Further, we found low levels of occupancy of CD63 and integrin α5β1. Together, these results demonstrated that NanoDeep can be implemented using expanded binder libraries that include several types of binders. NanoDeep has the potential to be a key tool in the investigation of the roles of higher-order association in EGFR family receptor signalling as well as in membrane receptor signalling in general.

Conclusions

We developed a method for analysing protein nanoenvironments at the cell membrane, called NanoDeep. A simple DNA nanoassembly with encoded spatial information is used to decipher the spatial organization of proteins at the cell membrane, which are labelled with oligo-conjugated binders. NanoDeep combines multiplexed deciphering capability with nanoscale spatial resolution, complementing the information obtainable with light-based super-resolution methods. Whereas NanoDeep provides ensemble averaged data over a cell population, super-resolution imaging enables discrete measurements of individual nanoenvironments and allows live imaging. NanoDeep provides high resolution information within a spatial range defined by the dimensions of the NanoComb, whereas long spatial ranges are analysed in super-resolution imaging. Both methods rely on the availability of specific, high affinity binders for analysing genetically unmodified cells. We showed that NanoDeep accommodates different types of binders, including affbodies, nanobodies, peptides and aptamers, which due to their small size do not limit the resolution of the method. The flexibility of NanoDeep regarding the types of binders facilitates further expansion of binder libraries. We applied NanoDeep to the analysis of the nanoenvironment surrounding the membrane protein Her2 and were able to simultaneously target six proteins. NanoDeep has the potential to enable a breakthrough in

the simultaneous analysis of the spatial distribution of many proteins at the membrane without microscopy measurements, providing a tool for understanding the importance of membrane protein assemblies.

Data availability

All data supporting the results of this study are available from the Swedish National Data Service (https://snd.gu/se/en).

Code availability

Codes for UMI processing and barcode association are available online at https://github.com/Intertangler/NanoDeep.

Additional Information

Supplementary Information is available in the online version of the paper. Reprints and permission information is available online at www.nature.com/reprints. Correspondence and requests for materials should be addressed to AIT.

References

1. Sengupta, P. et al. Probing protein heterogeneity in the plasma membrane using PALM and pair correlation analysis. *Nat. Methods* **8**, 969-975 (2011).
2. Bethani, I., Skånland, S. S., Dikic, I. & Acker-Palmer, A. Spatial organization of transmembrane receptor signalling. *EMBO J.* **29**, 2677-2688 (2010).
3. Rossier, O. et al. Integrins β1 and β3 exhibit distinct dynamic nanoscale organizations inside focal adhesions. *Nat. Cell. Biol.* **14**, 1057-1067 (2012).
4. Winckler, P. et al. Identification and super-resolution imaging of ligand-activated receptor dimers in live cells. *Sci. Rep.* **3**, 2387 (2013).
5. Garcia-Parajo, M. F., Cambi, A., Torreno-Pina, J. A., Thompson, N. & Jacobson, K. Nanoclustering as a dominant feature of plasma membrane organization. *J. Cell. Sci.* **127**, 4995-5005 (2014).
6. Sigal, Y. M., Zhou, R. & Zhuang, X. Visualizing and discovering cellular structures with super-resolution microscopy. *Science* **361**, 880-887 (2018).
7. Sahl, S. J., Hell, S. W. & Jakobs, S. Fluorescence nanoscopy in cell biology. *Nat. Rev. Mol. Cell Biol.* **18**, 685-701 (2017).
8. Jungmann, R. et al. Quantitative super-resolution imaging with qPAINT. *Nat. Methods* **13**, 439-442 (2016).
9. Jungmann, R. et al. Multiplexed 3D cellular super-resolution imaging with DNA-PAINT and Exchange-PAINT. *Nat. Methods* **11**, 313-318 (2014).
10. Klevanski, M. et al. Automated highly multiplexed super-resolution imaging of protein nano-architecture in cells and tissues. *Nat. Commun.* **11**, 1552 (2020).
11. Beghin, A. et al. Localization-based super-resolution imaging meets high-content screening. *Nat Methods* **14**, 1184-1190 (2017).
12. Dirks, R.M. & Pierce, N.A. Triggered amplification by hybridization chain reaction. *Proc Natl Acad Sci U S A* **101**, 15275-15278 (2004).
13. Söderberg, O. et al. Direct observation of individual endogenous protein complexes in situ by proximity ligation. *Nat. Methods* **3**, 995-1000 (2006).
14. Fredriksson, S. et al. Protein detection using proximity-dependent DNA ligation assays. *Nat. Biotechnol.* **20**, 473-477 (2002).
15. Hoffecker, I. T., Yang, Y., Bernardinelli, G., Orponen, P. & Högberg, B. A computational framework for DNA sequencing microscopy. *Proc. Natl. Acad. Sci. U S A* **116**, 19282-19287 (2019).
16. Weinstein, J. A., Regev, A. & Zhang, F. DNA Microscopy: Optics-free spatio-genetic imaging by a stand-alone chemical reaction. *Cell* **178**, 229-241.e216 (2019).

17. Boulgakov, A. A., Ellington, A. D. & Marcotte, E. M. Bringing microscopy-by-sequencing into view. *Trends Biotechnol.* (2019).
18. Rubin, I. & Yarden, Y. The basic biology of HER2. *Ann. Oncol.* **12 Suppl 1**, S3-8 (2001).
19. Yarden, Y. Biology of HER2 and its importance in breast cancer. *Oncology* **61 Suppl 2**, 1-13 (2001).
20. Yarden, Y. & Sliwkowski, M. X. Untangling the ErbB signalling network. *Nat. Rev. Mol. Cell Biol.* **2**, 127-137 (2001).
21. Peckys, D. B., Korf, U. & de Jonge, N. Local variations of HER2 dimerization in breast cancer cells discovered by correlative fluorescence and liquid electron microscopy. *Sci. Adv.* **1**, e1500165 (2015).
22. Stove, C. & Bracke, M. Roles for neuregulins in human cancer. *Clin. Exp. Metastasis* **21**, 665-684 (2004).
23. Ho-Pun-Cheung, A. et al. Quantification of HER expression and dimerization in patients' tumor samples using time-resolved Förster resonance energy transfer. *PLoS One* **7**, e37065 (2012).
24. Weitsman, G. et al. HER2-HER3 dimer quantification by FLIM-FRET predicts breast cancer metastatic relapse independently of HER2 IHC status. *Oncotarget* **7**, 51012-51026 (2016).
25. Claus, J. et al. Inhibitor-induced HER2-HER3 heterodimerisation promotes proliferation through a novel dimer interface. *Elife* **7** (2018).
26. Jeon, M. et al. Dimerization of EGFR and HER2 induces breast cancer cell motility through STAT1-dependent ACTA2 induction. *Oncotarget* **8**, 50570-50581 (2017).
27. Kaufmann, R., Müller, P., Hildenbrand, G., Hausmann, M. & Cremer, C. Analysis of Her2/neu membrane protein clusters in different types of breast cancer cells using localization microscopy. *J. Microsc.* **242**, 46-54 (2011).
28. Iqbal, N. Human Epidermal Growth Factor Receptor 2 (HER2) in Cancers: Overexpression and Therapeutic Implications. *Mol. Biol. Int.* **2014**, 852748 (2014).
29. Needham, S. R. et al. EGFR oligomerization organizes kinase-active dimers into competent signalling platforms. *Nat. Commun.* **7**, 13307 (2016).
30. Hiroshima, M. et al. Transient acceleration of Epidermal Growth Factor Receptor dynamics produces higher-order signaling clusters. *J. Mol. Biol*. **430**, 1386-1401 (2018).
31. Liang, S. I. et al. Phosphorylated EGFR dimers are not sufficient to activate Ras. *Cell. Rep.* **22**, 2593-2600 (2018).
32. van Lengerich, B., Agnew, C., Puchner, E. M., Huang, B. & Jura, N. EGF and NRG induce phosphorylation of HER3/ERBB3 by EGFR using distinct oligomeric mechanisms. *Proc. Natl. Acad. Sci. U S A* **114**, E2836-E2845 (2017).
33. Baumann, C. G., Smith, S. B., Bloomfield, V. A. & Bustamante, C. Ionic effects on the elasticity of single DNA molecules. *Proc. Natl. Acad. Sci. U S A* **94**, 6185-6190 (1997).
34. Bernardinelli, G. & Högberg, B. Entirely enzymatic nanofabrication of DNA-protein conjugates. *Nucleic Acids Res.* **45**, e160 (2017).
35. Yurke, B., Turberfield, A. J., Mills, A. P., Simmel, F. C. & Neumann, J. L. A DNA-fuelled molecular machine made of DNA. *Nature* **406**, 605-608 (2000).
36. Xu, H. et al. Enhanced DNA toehold exchange reaction on a chip surface to discriminate single-base changes. *Chem. Commun.* **50**, 14171-14174 (2014).
37. Tan, M., Grijalva, R. & Yu, D. Heregulin beta1-activated phosphatidylinositol 3-kinase enhances aggregation of MCF-7 breast cancer cells independent of extracellular signal-regulated kinase. *Cancer Res.* **59**, 1620-1625 (1999).
38. Breuleux, M. Role of heregulin in human cancer. *Cell Mol. Life Sci.* **64**, 2358-2377 (2007).
39. Yang, C., Klein, E. A., Assoian, R. K. & Kazanietz, M. G. Heregulin beta1 promotes breast cancer cell proliferation through Rac/ERK-dependent induction of cyclin D1 and p21Cip1. *Biochem. J.* **410**, 167-175 (2008).
40. Atlas, E. et al. Heregulin is sufficient for the promotion of tumorigenicity and metastasis of breast cancer cells in vivo. *Mol. Cancer Res.* **1**, 165-175 (2003).

41. Huang, Y. et al. Molecular basis for multimerization in the activation of the epidermal growth factor receptor. *Elife* **5** (2016).
42. Desgrosellier, J. S. & Cheresh, D. A. Integrins in cancer: biological implications and therapeutic opportunities. *Nat. Rev. Cancer* **10**, 9-22 (2010).
43. Stoeltzing, O. et al. Inhibition of integrin alpha5beta1 function with a small peptide (ATN-161) plus continuous 5-FU infusion reduces colorectal liver metastases and improves survival in mice. *Int. J. Cancer* **104**, 496-503 (2003).
44. Khalili, P. et al. A non-RGD-based integrin binding peptide (ATN-161) blocks breast cancer growth and metastasis in vivo. *Mol. Cancer Ther.* **5**, 2271-2280 (2006).
45. Kuwada, S. K., Kuang, J. & Li, X. Integrin alpha5/beta1 expression mediates HER-2 down-regulation in colon cancer cells. *J. Biol. Chem.* **280**, 19027-19035 (2005).
46. Wang, S. E. et al. Transforming growth factor beta induces clustering of HER2 and integrins by activating Src-focal adhesion kinase and receptor association to the cytoskeleton. *Cancer Res.* **69**, 475-482 (2009).
47. Pols, M. S. & Klumperman, J. Trafficking and function of the tetraspanin CD63. *Exp. Cell. Res.* **315**, 1584-1592 (2009).
48. Khushman, M. et al. Exosomal markers (CD63 and CD9) expression and their prognostic significance using immunohistochemistry in patients with pancreatic ductal adenocarcinoma. *J Gastrointest. Oncol.* **10**, 695-702 (2019).
49. Ng, Y. H. et al. Endometrial exosomes/microvesicles in the uterine microenvironment: a new paradigm for embryo-endometrial cross talk at implantation. *PLoS One* **8**, e58502 (2013).
50. de Goeij, B. E. et al. Efficient payload delivery by a bispecific antibody-drug conjugate targeting HER2 and CD63. *Mol. Cancer. Ther.* **15**, 2688-2697 (2016).
51. Livant, D. L. et al. Anti-invasive, antitumorigenic, and antimetastatic activities of the PHSCN sequence in prostate carcinoma. *Cancer Res.* **60**, 309-320 (2000).
52. Maier, K. E. et al. A new transferrin receptor aptamer inhibits new world hemorrhagic fever mammarenavirus entry. *Mol. Ther. Nucleic Acids* **5**, e321 (2016).
53. Porciani, D. et al. Modular cell-internalizing aptamer nanostructure enables targeted delivery of large functional RNAs in cancer cell lines. *Nat. Commun.* **9**, 2283 (2018).

Acknowledgements

The authors acknowledge Björn Reinius for helpful discussions and Simone Dal Zilio for the development and fabrication of micropatterned surfaces, performed at the Facility of Nano Fabrication FNF-IOM, CNR, Trieste. A.I.T. acknowledges support from the European Research Council under the European Union's Seventh Framework Programme (ERC, grant no. 617711), the Swedish Research Council (grant no. 2015-03520) and the Knut and Alice Wallenberg Foundation (grant no. KAW 2017.0114).

Authors contributions

E.A. designed the study and performed the experiments; G.B. designed the affibodies plasmids; G.B. and B.H. provided key insights for the design of experiments; I.H developed NGS data analysis; L.H and R.S. contributed to performance and interpretation of NGS experiments; G.K and A.dM. contributed to the development of expanded library. A.I.T. conceived and supervised the study; E.A. and A.I.T. wrote the manuscript, with input from all authors; all authors contributed to the manuscript revision and gave approval to the final version.

Competing interests

The authors declare no competing interests.

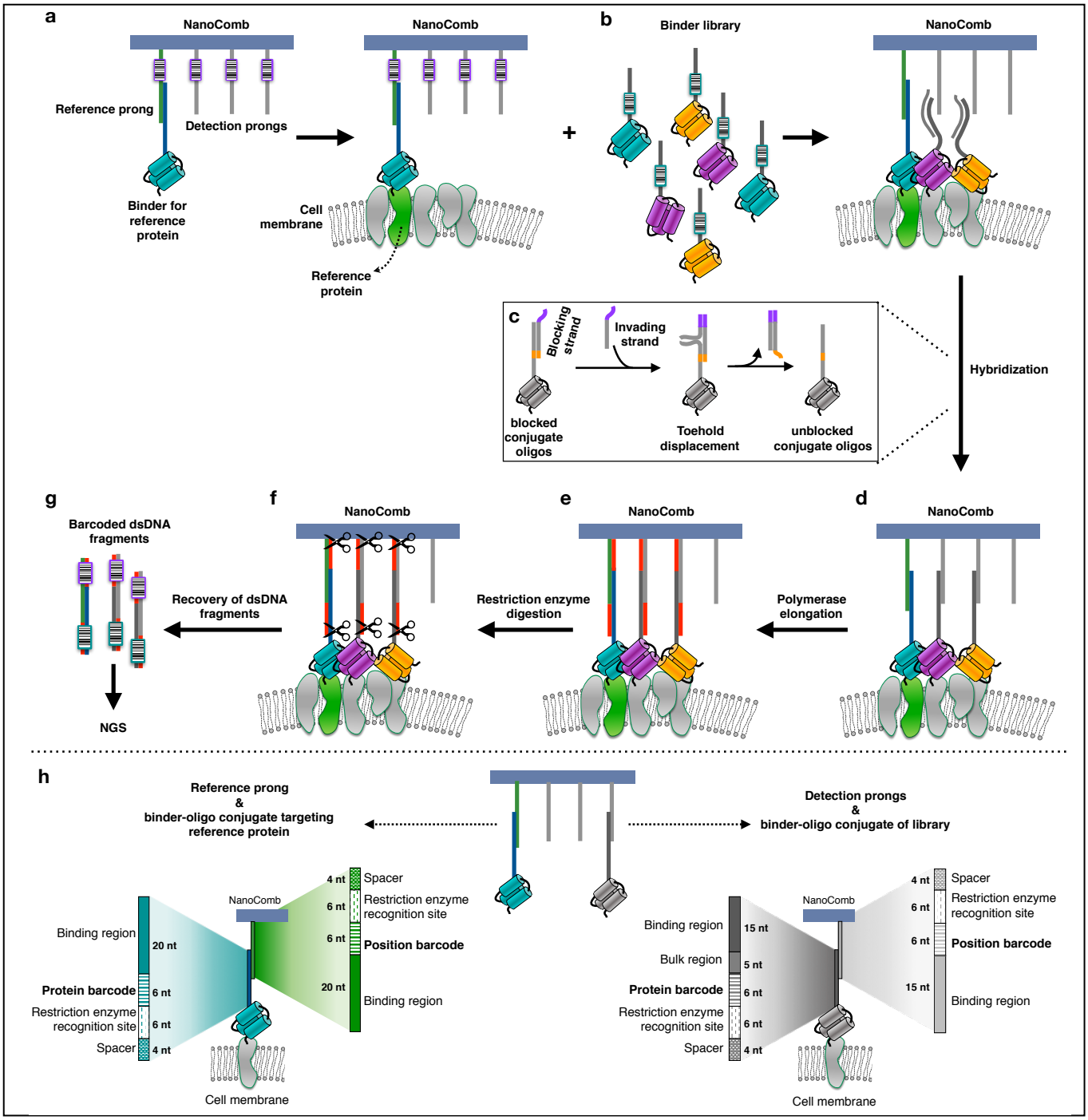

Fig. 1: Schematic of the NanoDeep method. a, A DNA nanoassembly (NanoComb) consisting of a double stranded backbone with four barcoded protruding ssDNA strands (prongs) is preloaded with an oligo-conjugated binder specific for the reference protein and incubated with fixed cells. **b,** A library of binders is added, each conjugated to a ssDNA sequence bearing a barcode that identifies its target protein as well as a sequence that is partially complementary to the sequences of the detection prongs. **c,** During the incubation, affibody-oligo conjugates are hybridized with a blocking strand. Unblocking is promoted by toehold-mediated displacement guided by an invading strand. **d,** The free 3' ends formed by the hybridization of the prongs with the binder oligos function as primers for DNA polymerase. **e,** DNA polymerase reaction creates dsDNA sequences that contain both the barcodes for the relative position of the prongs within the NanoComb and for the protein that is recognized by the binder. **f,** Restriction enzymes cleave the dsDNA sequences at specific nuclease target sequences that are included in both the prongs and the binder oligos, leading to the release of dsDNA sequences. **g,** dsDNA sequences are analysed by NGS. **h,** Schematic representation of prongs and oligos conjugated to the binders, which contain binding regions complementary to each other. For the reference prong and the oligo conjugated to the binder targeting the reference protein (left) this region is 20-nucleotides (nt) long. For detection prongs and the oligos conjugated to the library binders (right) the binding region is 15-nt long; a 5-nt long bulk region is added to the oligo sequences of the conjugates. Binding regions are followed by a 6-nt barcode identifying the protein or the position, in the binder oligos or the prongs, respectively. Further, both the prongs and the binder oligos contain nuclease target sites (6-nt) followed by a 4-nt spacer, included to facilitate the binding of the restriction enzyme.

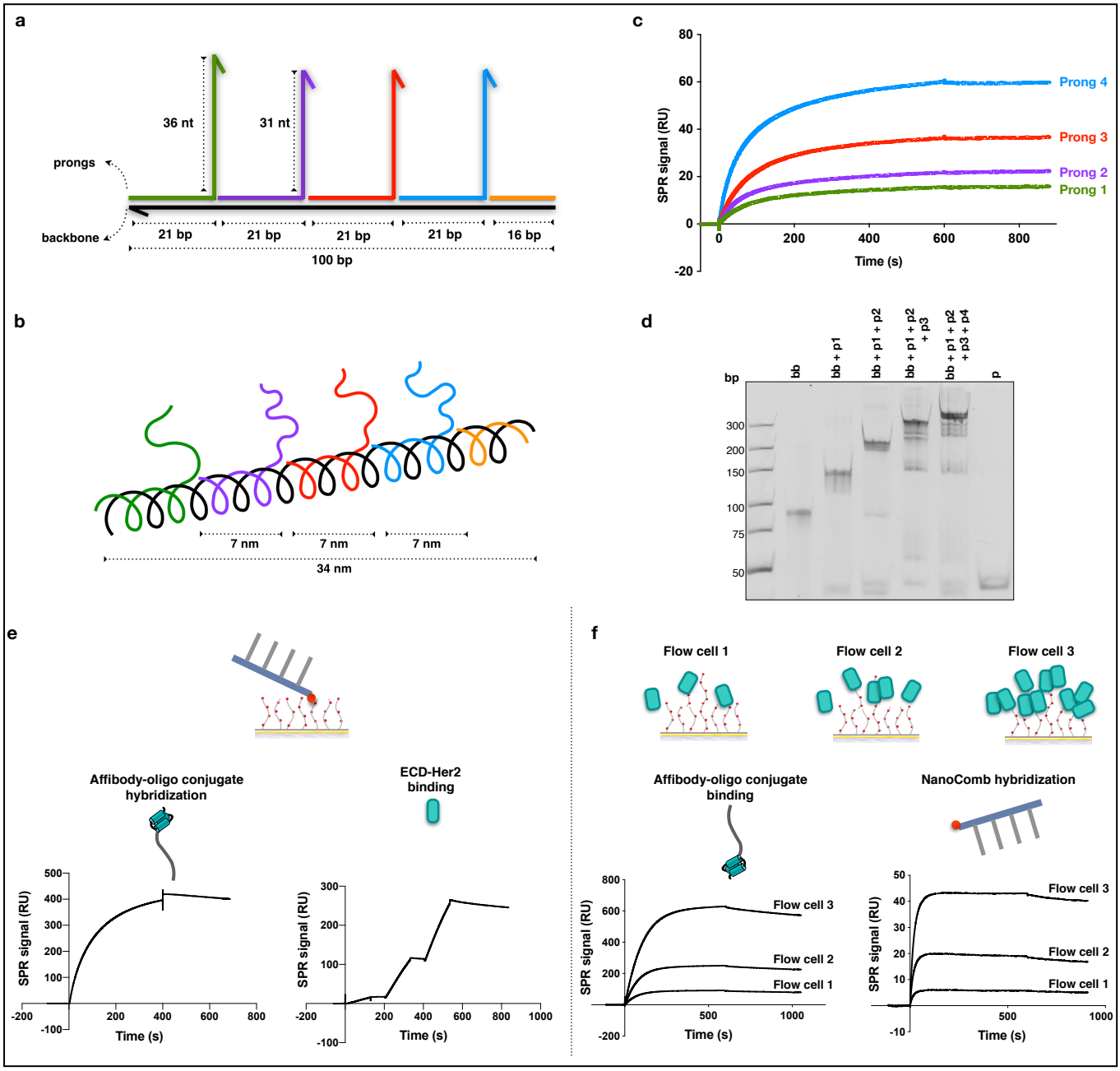

Fig. 2: NanoComb characterisation. a, NanoComb composed of a 100-nt ssDNA backbone and four 57- or 52-nt ssDNA strands (reference and detection prongs, respectively), each of which hybridizes to the backbone by means of the first 21-nt, leaving the remaining 36- or 31-nt ssDNA sequences to protrude from the backbone. **b,** In an extended DNA conformation, the total length of NanoComb is 34 nm and the prongs protrude from the backbone with a period of 21 bp, which corresponds to a distance of 7 nm, along the helical direction of the backbone. **c,** Real time kinetic analysis using SPR of sequential binding of the prongs to the backbone, which was immobilised onto the SPR sensor surface. RU, resonance units. **d,** The backbone alone (bb) or the backbone hybridised with one (bb+p1), two (bb+p1+p2), three (bb+p1+p2+p3) or all four prongs (bb+p1+p2+p3+p4), monitored by native PAGE (7%). One prong sequence was loaded as a control (p). **e, f,** The incorporation of affibody-oligo conjugates in the NanoCombs was verified using direct (e) and reverse (f) SPR assays. In the direct assay (e), we measured the hybridization of affibody-oligo conjugates to desthiobiotinylated NanoCombs immobilised on Streptavidin (SA) SPR surfaces, followed by measurement of ECD-Her2 binding, to verify that the affibodies preserved their ability to recognize Her2. In the reverse assay (f), ECD-Her2 was covalently immobilised on the sensor surface at three different surface densities. Sensorgrams showed sequential binding of affibody-oligo conjugates and of NanoCombs. The SPR signal obtained from NanoComb binding to the affibody-oligo conjugates was proportional to the amount of bound conjugates, which in turn reflected the surface density of ECD-Her2.

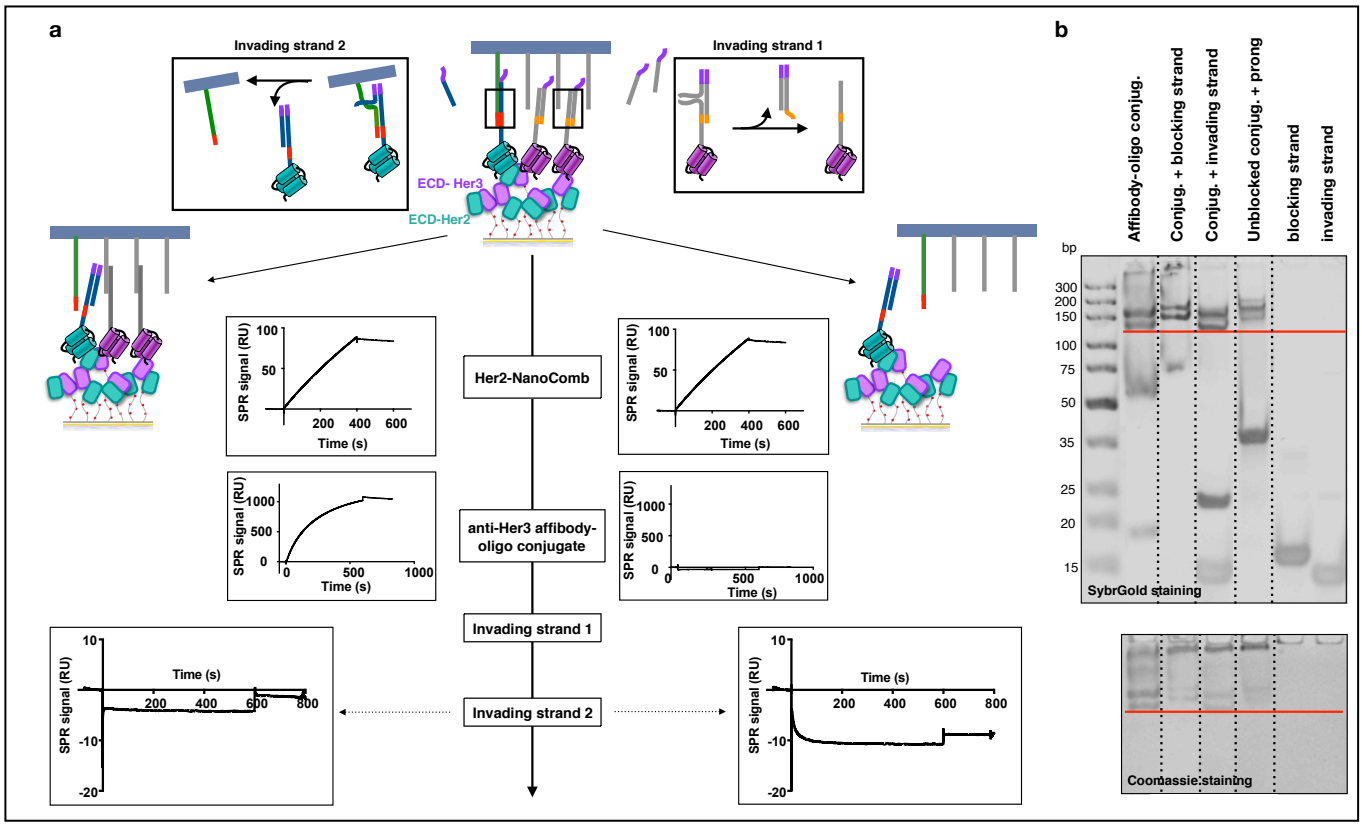

Fig. 3: Toehold exchange reversibly blocked the hybridization of affibody-oligo conjugates to the NanoCombs. a, A 1:1 mixture of ECD-Her2 and ECD-Her3 was covalently attached to the SPR surfaces of two separate flow cells. Her2-NanoCombs were injected and binding to the anchored ECD-Her2 was detected by an increase in the sensorgram signal. Anti-Her3 affibody-oligo conjugates, previously hybridised with a blocking strand, were added to flow cell 1 (on the left) but not to flow cell 2 (on the right). In flow cell 1, a first invading strand (invading strand 1) was injected, promoting unblocking of the anti-Her3 affibody-oligo conjugates and hybridization to the detection prongs of the NanoComb. Importantly, we performed this step after increasing the temperature to 45 °C, which is below the melting temperature of the hybridization between the invading strand and the blocking strand but above the melting temperature of the hybridization between the invading strand and the prongs. This prevented the hybridization of invading strand to the prongs of the NanoCombs. Temperature was then decreased to 25 °C and the oligo tails of the affibody-oligo conjugates were then free to hybridize to the detection prongs of the NanoCombs. The sequences of the anti-Her2 conjugates preloaded on the reference prong contained an added 7-nt at 3' end in this experiment. This allowed for a second toehold exchange reaction that promoted the displacement of anti-Her2 conjugates from the reference prong. This caused a larger decrease in the SPR signal in flow cell 2, where binding of the NanoComb to the surface is mediated only by the reference prong (bottom-right), than in cell flow 1, where the NanoComb remains bound to the surface through the interaction of the detection prongs with the anti-Her3 conjugates (bottom-left). **b,** EMSA using native PAGE (13%) was performed on samples that underwent blocking/unblocking reactions in solution. The hybridization of blocking strand to affibody-oligo conjugate was visualised by a shift of the conjugate band (the red line indicates the level without blocking). Displacement of the blocking strand by the invading strand was visualised by a shift in the conjugate band and the presence of the released dsDNA fragment consisting of the blocking strand hybridised to the invading strand. We observed a further shift in the conjugate band when adding the complementary prong.

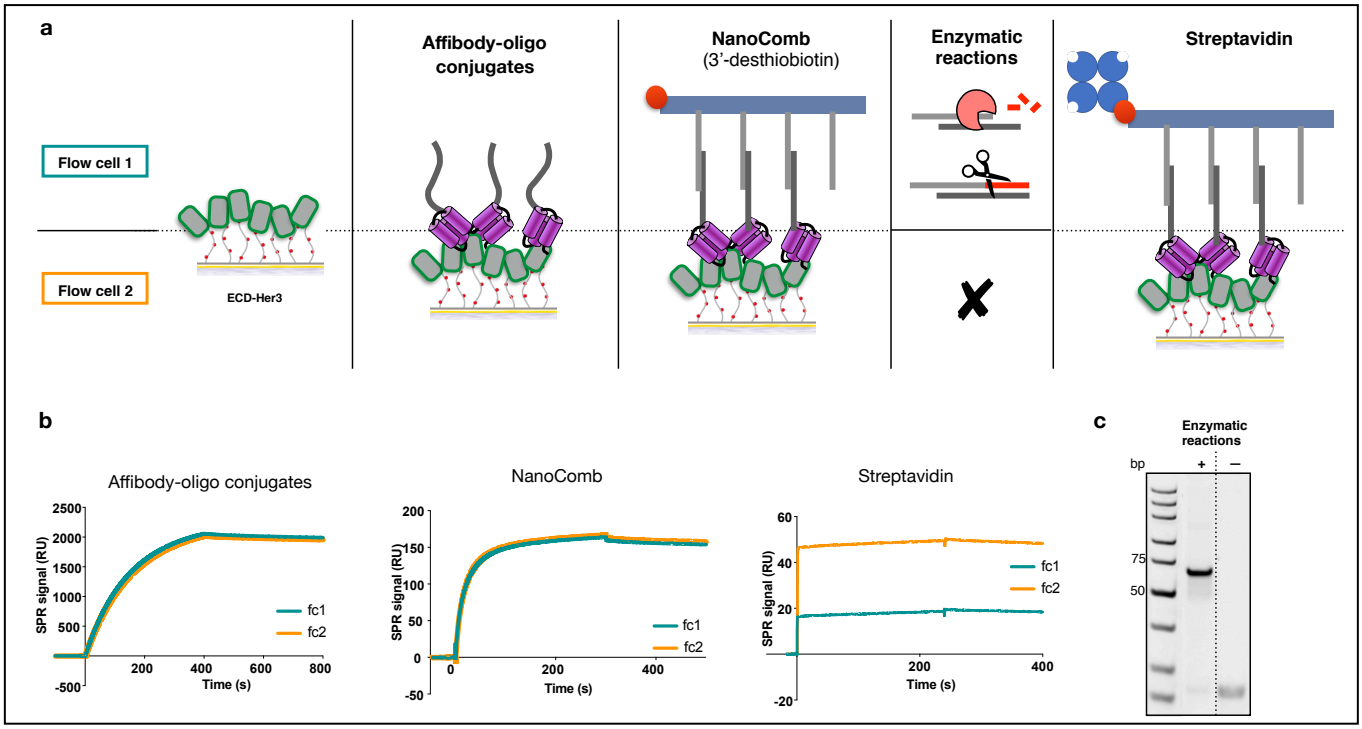

Fig. 4: DNA polymerase and nuclease reactions generated barcoded dsDNA sequences. a, Schematic representation of the SPR assay; equivalent amounts of ECD-Her3 were covalently attached to two SPR flow cells. Anti-Her3 affibody-oligo conjugates bound first to the target proteins and then hybridised with the NanoCombs. To promote the release of the barcoded dsDNA sequences, T4 polymerase DNA elongation and restriction enzyme cleavage were performed. The enzymatic reactions were carried out only on flow cell 1 and flow cell 2 was used as a negative control. Finally, streptavidin that is able to bind to the desthiobiotin on 3' end of NanoComb backbone, was injected over the two flow cells to detect the residual amounts of NanoCombs remaining on the surface. **b,** SPR signals of the conjugates and NanoCombs were comparable on the two flow cells. The binding of streptavidin was significantly reduced in flow cell 1 compared to flow cell 2, demonstrating the efficiency of the enzymatic reactions. **c,** Barcoded dsDNA sequences visualised on native PAGE (13%) after PCR amplification were recovered from flow cell 1 but not from the negative control, flow cell 2.

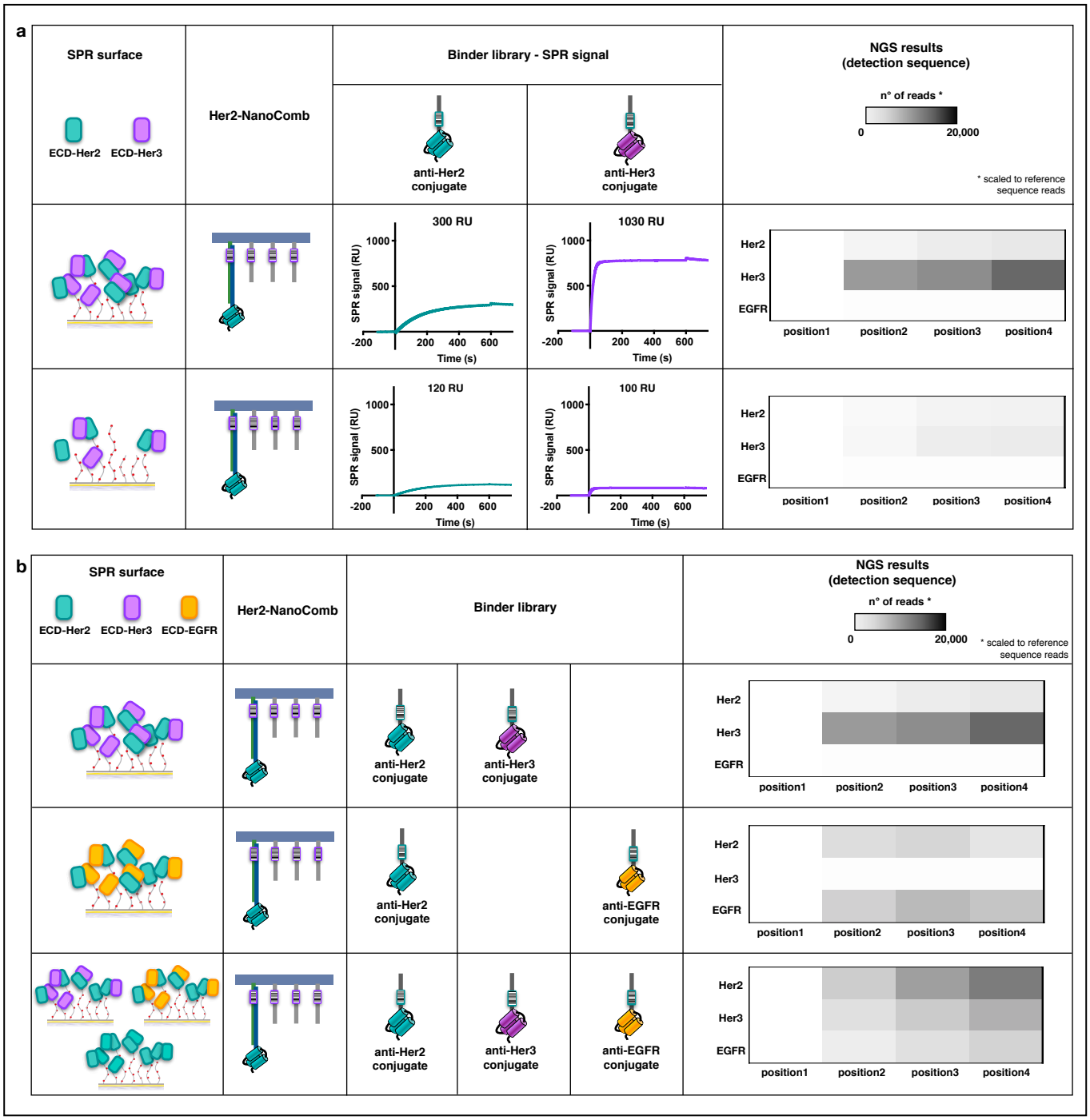

Fig. 5: NanoDeep on model SPR surfaces. a, 1:1 mixtures of ECD-Her2 and ECD-Her3 were covalently attached to the SPR surfaces of two sensor chips at two different surface densities. NanoDeep was performed by first flowing Her2-NanoCombs and then binder libraries consisting of anti-Her2 and anti-Her3 conjugates. Binding to the anchored proteins was monitored by sensorgram signals, which reflect the amount of anchored proteins. NGS analyses were performed in duplicate and presented as mean values in the heatmap. Barcode reads from the detection sequences were scaled to the reference sequence reads. **b,** NanoDeep was performed on SPR surfaces presenting different compositions of EGFR family receptors: Her2-Her3 (top), Her2-EGFR (middle) and a 1:1:1 mixture of Her2-Her2, Her2-Her3 and Her2-EGFR (bottom). NGS analyses were performed in duplicate and presented as mean values in the heatmap.

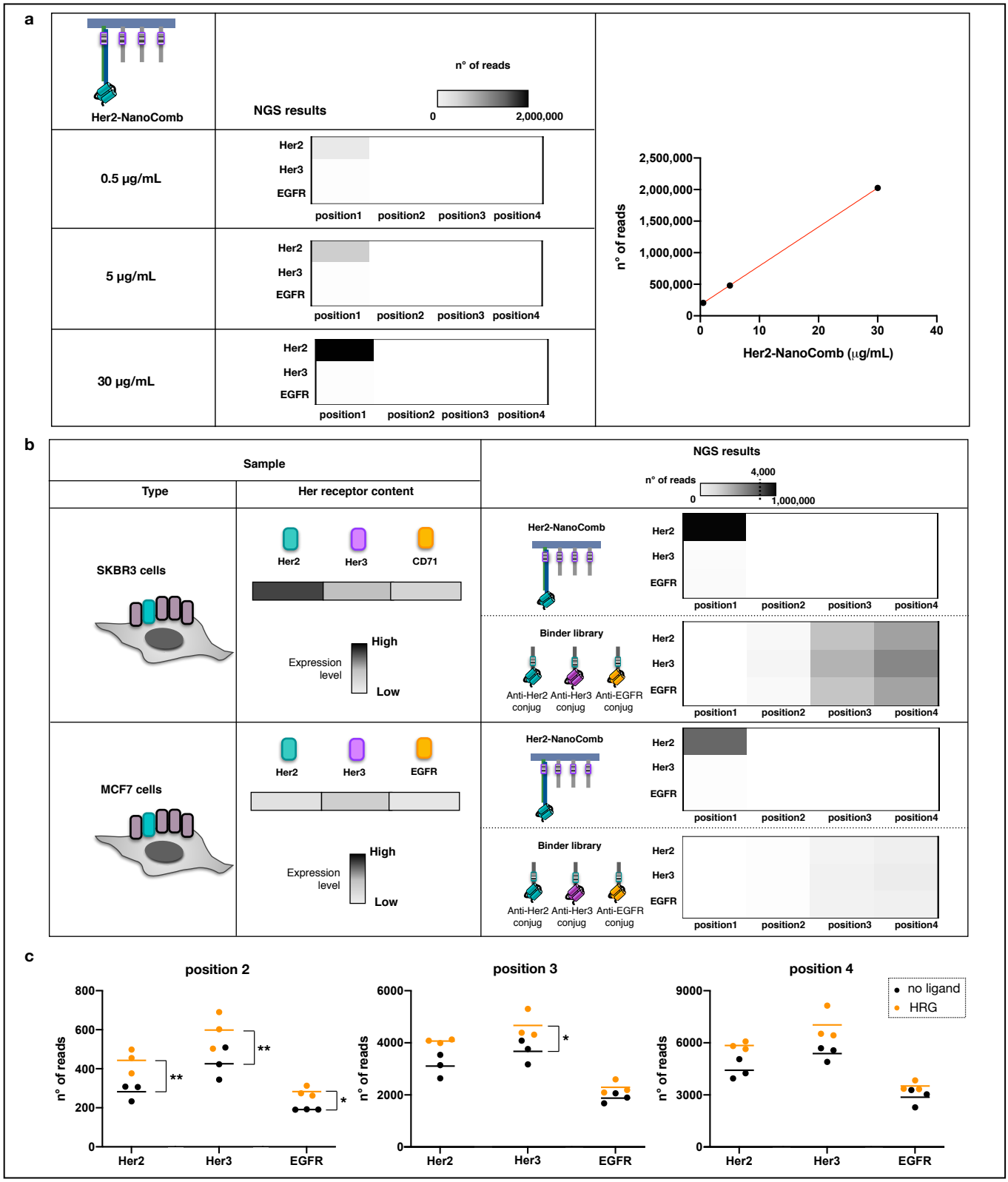

Fig. 6: NanoDeep on cells. a, NGS analysis revealed a linear correlation between NGS reads and the concentration of Her2-NanoCombs. SKBR3 cells were treated with three different concentrations of Her2-NanoCombs: 0.5 µg/mL, 5 µg/mL and 30 µg/mL. NGS reads are presented in heatmaps (left panel) and as a plot showing a linear correlation between the number of NGS reads of reference sequences and NanoComb concentrations (right panel). **b,** SKBR3 cells and MCF7 cells were grown to similar densities and analysed by NanoDeep using Her2-NanoCombs and anti-Her2, -Her3 and -EGFR binder libraries. All measurements were performed in triplicate and presented as mean values in two types of heatmaps, showing the reads from the reference sequences (top) and detection sequences (bottom). **c,** SKBR3 cells were starved for 24 h and then stimulated for 15 min with HRG-β1, followed by NanoDeep assay. Untreated cells were used as controls. For each position of the NanoComb, the number of reads of detection sequences was plotted versus the protein identity barcodes, for HRG-β1 treated cells (orange dots) and control cells (black dots). Dots represent three independent experiments and lines represent means of each condition. *p≤0.05; **p≤0.01.

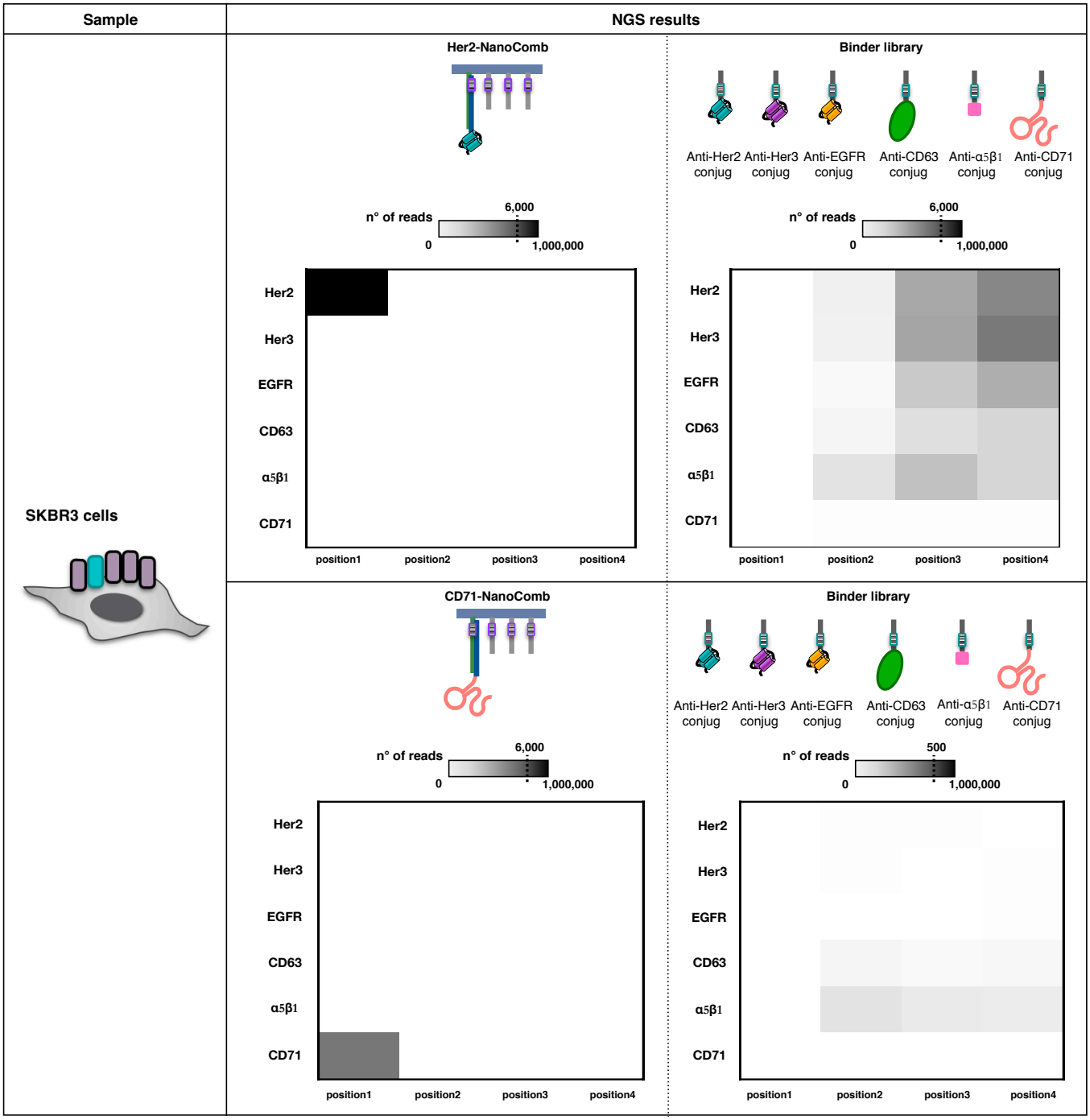

Fig. 7: NanoDeep with expanded library. NanoDeep was performed on SKBR3 cells using Her2-NanoCombs (top) or CD71-Nanocombs (bottom) and anti-Her2, -Her3, -EGFR, CD63, α5β1 and CD71 binder libraries. All measurements were performed in triplicate and presented as mean values in two types of heatmaps, showing the reads from the reference sequences (left) and detection sequences (right).

Methods

DNA sequences

All synthetic DNA sequences were obtained from Integrated DNA Technologies, except for the AbCodeCD63_library sequence which was obtained from Biomers.net. DNA sequence details are reported in the Supplementary Information (Supplementary Table 1).

Folding, purification and electrophoretic characterisation of DNA NanoCombs

Backbone and protruding strands (prongs) ssDNA sequences were diluted at a concentration of 1 µM and 2 µM, respectively, in Hybridization Buffer (5 mM Tris-HCl pH 8.0, 10 mM $MgCl_2$, 1 mM EDTA). Folding

was carried out by rapid heat denaturation (80 °C for 10 min) followed by cooling to RT for 2 h. Removal of excess prongs was done first with washing in 50 kDa MWCO 0.5 mL Amicon centrifugal filters (Merck Millipore) and then by means of Streptavidin-coated magnetic beads (DYNAL MyOne Dynabeads Streptavidin C1- Thermofisher Scientific) as follows: beads were washed with PBS and then with Immobilization Buffer (5 mM Tris-HCl pH 7.5, 1 M NaCl, 0.5 mM EDTA). NanoCombs were incubated with beads at RT for 1 h; beads were then collected with a magnet and the supernatant was discarded. The elution of NanoCombs from beads was performed with 5 mM biotin (Invitrogen) for 30 min at RT. Native polyacrylamide gels were stained with SybrGold to visualize the NanoComb stepwise assembly (7%) and the purification yield (13%).

Design, expression and purification of affibody-VirD2 fusion proteins

The coding sequences of anti-Her2 ($Z_{Her2:34}$[1]), anti-Her3 (Z_{08699}[2]) and anti-EGFR ($Z_{EGFR:2377}$[3]) affibodies were synthetised (BioCat) and cloned (XhoI/BamHI) at the C-terminal of the VirD2 protein connected via a flexible linker (GGGGS) in the expression plasmid pET-16-b and the sequences were validated by sequencing. Expression and purification of recombinant proteins were carried out as previously described[4] at the Karolinska Institutet/SciLifeLab Protein Science Core Facility.

VirD2 tag mediated conjugation of oligonucleotides to affibodies and purification of conjugates

For the conjugation reaction, protein and oligonucleotide were mixed at a 1:0.75 ratio in TKM buffer (50 mM Tris-HCl pH 8, 150 mM KCl, 1 mM $MgCl_2$, 10% glycerol) and incubated at 37 ºC for 2 h. Conjugates were then purified from the excess oligo and the fraction of protein not conjugated by isolation from a native PAGE gel. Briefly, conjugates were separated from oligos and excess protein by electrophoresis by native PAGE (10%). The bands corresponding to the conjugates were cut and incubated overnight at 4 °C in TBS buffer (50 mM Tris-HCl pH 7.5, 150 mM $MgCl_2$). Buffer with eluted conjugates was finally filtrated with Nylon 0.45 μM centrifugal filter (Thermofisher Scientific).

Anti-CD63 binder-oligo conjugate production

A recombinant nanobody was previously selected during a panning performed using directly extracellular vesicles and its characterisation indicated that it recognizes a major Extracellular Vesicles (EV) biomarker largely conserved in vesicles recovered from different sources[5]. We confirmed by SPR experiments high affinity binding for EV biomarker CD63. The original sequence was subcloned, fused to the SpyTag, as previously described[6], to be used in combination with SpyCatcher[7]. Expression and purification of recombinant SpyCatcher protein with N-terminal cysteine were carried out at the Karolinska Institutet/SciLifeLab Protein Science Core Facility. pDEST14-Cys-SpyCatcher002[8-11] was a gift from Mark Howarth (Addgene plasmid #102829; http:// n2t.net/addgene:102829; RRID:Addgene_102829). SpyCatcher was first conjugated to an oligo sequence by means of maleimide reaction: SpyCatcher was diluted to a concentration of 100 μM in Hepes 10 mM pH 7.0 buffer and kept reduced by the addition of TCEP in 10-fold molar excess for 20 minutes at RT. The oligo sequence was dissolved in TE buffer (Tris 10 mM, EDTA 1 mM, pH 8.0) and then added to SpyCatcher with a molar ratio of DNA to protein of 10:1 (250:25 μM:μM). After 2 h at RT the modified SpyCatcher was purified by Pierce Strong Ion Exchange Spin Columns (Thermofisher Scientific). SpyCatcher-oligo complex was then incubated with SpyTag-nanobody with a molar ratio SpyCatcher-oligo:SpyTag-nanobody of 2:1 in PBS pH 7.6 for 2 h at RT. Anti-CD63 binder-oligo conjugate was finally purified by means of 30 kDa MWCO 0.5 mL Amicon centrifugal filters.

Anti-integrin α5β1 binder-oligo conjugate production

The conjugation of anti-integrin α5β1 peptide ATN-161 with the DNA oligo was performed by means of click chemistry reaction exploiting the commercial Protein-Oligo Conjugation Kit according to the manufacturers' instructions (SoluLink). The conjugation reaction was visualised spectrophotometrically by determining the absorbance at A354 due to the formation of the chromophoric conjugate bond. The reaction solution was exchanged in PBS using 7K Zeba columns.

Anti-CD71 binder-oligo conjugate production

Anti-CD71 RNA aptamer was generated via in vitro run-off transcription. A T7 RNA polymerase promoter sequence (underlined) and AbCodeCD71_NC or AbCodeCD71_library sequences (in bold) were added to the anti-CD71 aptamer sequence to generate the template (5' GAA TTC TAA TAC GAC TCA CTA TAG GGG GGT TCT ACG ATA AAC GGT TAA TGA CCA GCT TAT GGC TGG CAG TTC CC**T TTT GGA TCC TTA GGG GCA TCC ACT CAT TCA ATA CC** 3'). In vitro run-off transcription reaction was performed using Durascribe T7 transcription kit (Lucigen). Briefly, the DNA template and its complementary sequence were first diluted in annealing buffer (30 mM Hepes, 100 mM Potassium Acetate, pH 7.5) and heated at 95 °C for 3 min. Annealing step was performed at RT for 30 min. 1 μg of dsDNA template was added to 400 U of T7 RNA polymerase (Y639F mutant), 5 mM 2'-fluoro-modified CTP, 5 mM 2'-fluoro-modified UTP, 5 mM ATP, 5 mM GTP, 10 mM DTT in RNase-free distilled water. This reaction solution was incubated for 4 h at 37 °C and then treated with RNase-Free DNase I for 15 min at 37 °C. Aptamer-oligo was finally purified with RNA Clean & Concentrator-25 (Zymo Research) according to the manufacturer's instructions.

Functionalization of NanoCombs with anti-Her2, anti-Her3 and anti-CD71 affibody-oligo conjugates on reference prong (Her2-, Her3- and CD71-NanoCombs)

NanoCombs were folded and loaded on Streptavidin-coated magnetic beads, as previously described. Anti-Her2/anti-Her3 affibodies or anti-CD71 aptamer, conjugated with an oligo sequence that partially hybridizes to the reference prong and purified as described above, were incubated with the beads at RT for 2 h. Beads were then collected with a magnet and the supernatant was discarded. Finally, Her2-, Her3- and CD71-NanoCombs were eluted from the beads with 5 mM biotin for 30 min at RT.

Surface Plasmon Resonance assays

Biacore T200 instrument and related reagents (GE Healthcare) were used to perform all SPR experiments. *NanoComb assembly characterisation.* SA gold sensor chip was used to immobilize desthiobiotinylated-backbone DNA sequence (ligand) and to verify the hybridization of the protruding strands (analyte). HBS-EP+ was used as running buffer. *Binding/kinetics of VirD2-affibodies and affibody-oligo conjugates.* ECD-Her2/-Her3/-EGFR proteins (AcroBiosystem), were immobilised on CM3 or CM5 sensor chip via amine coupling reactions, according to the manufacturers' instructions. Binding affinity tests of the VirD2-affibodies and affibody-oligo conjugates were performed by injecting different concentrations of analytes in running buffer (HBS-EP+). The surface was regenerated with Gly-HCl pH 2.0 solution. The dissociation equilibrium constant (K_D), the association rate constant (k_{on}), and the dissociation rate constant (k_{off}) were determined using the BIAevaluation 3.0 software, assuming a 1:1 binding model. *Characterisation of the binding between conjugates and NanoCombs.* Desthiobiotinylated-NanoCombs were immobilised on SA gold sensor chips. Then affibody-oligo conjugates (targeting Her2) were injected over the surface at 1 μM. The binding capability of Her2 was verified by flowing three increasing concentrations of ECD-Her2 (0.5-5-50 nM) in single cycle kinetic mode. In the reverse assay, ECD-Her2 was covalently immobilised on CM3 sensor chips, reaching three different surface densities on independent flow cells. Next, anti-Her2 affibody-oligo conjugates (at 50 nM) and NanoCombs (at 400 nM) were sequentially flowed over the surface. HBS-EP+ buffer was used as running buffer. *Toehold exchange strategy.* Assay 1: Binder oligos corresponding to the DNA sequences of the affibody-oligo conjugates, biotinylated at the 5' end, were immobilised on SA sensor chips. Blocking strand oligos were injected at the concentration of 1 μM; the displacement of blocking oligo by branch migration was promoted by injection of 2 μM of invading strands over the surface. After that, a partially assembled NanoComb (backbone + prong 2 and prong 3) at 2 μM concentration was allowed to interact with the unblocked immobilised oligos. TE/Mg^{2+} buffer (10 mM Tris pH 8.0, 12.5 mM $MgCl_2$,1 mM EDTA) was used as running buffer. Assay 2: ECD-Her2 and ECD-Her3 were mixed 1:1 and incubated for 1 h. Then they were injected over a CM5 sensor surface (two flow cells) for covalent immobilization. Her2-NanoCombs were injected over the surface and then anti-Her3 affibody-oligo conjugates, previously hybridised with blocking strand, were injected over only one of the two active flow cells. The blocking strand was then displaced by injection of invading strand 1; during this step the temperature was increased to 45 °C to prevent hybridization of invading strand to the detection prongs. Temperature was decreased to 25 °C and the system was left in stand-by mode for 1 h to allow hybridization of oligos of the conjugates to the detection prongs.

After that, invading strand 2 was injected over the surface. HBS-EP+ buffer was used as running buffer. *Validation of enzymatic reactions.* ECD-Her3 was covalently immobilised on two flow cells of CM5 sensor chip, reaching the same immobilization level. Anti-Her3 affibody-oligo conjugates were injected over the surface, followed by injection of NanoCombs in HBS-EP+ as running buffer. After that, T4 polymerase (New England BioLabs) at 15 units/mL was injected over the flow cell 1 in Neb2.1 buffer 1x (New England BioLabs) for 15 min at 12 °C. Then, first EcoRI (New England BioLabs) and afterwards BamHI (New England BioLabs), at 15 units/mL, were injected over the flow cell 1 in Neb2.1 buffer 1x and Cut Smart buffer 1x (New England BioLabs) respectively, for 15 min at 37 °C. Finally, running buffer was changed back to HBS-EP+ to perform the injection of Streptavidin over both flow cells 1 and 2. *Binding/kinetic of Her2-and Her3-NanoComb.* 1:1 mixtures of ECD-Her2 and ECD-Her3 were covalently attached to the SPR surfaces, on CM5 sensor chips. Binding of Her2- and Her3-NanoCombs was performed by injecting increasing concentrations in single cycle kinetic mode. Fitting was performed using a 1:1 kinetic model to determine the dissociation constant, K_D. *NanoDeep experiment.* Different sensor surfaces were created by covalently immobilizing ECD-Her2/-Her3/-EGFR alone or in different combinations on CM5 chip. Her2-NanoCombs were injected over the surface. After that, libraries of affiboby-oligo conjugates, previously hybridised with blocking strand, were injected. Toehold-mediated strand displacement and enzymatic reactions were performed as previously described. The digestion products of BamHI were recovered in a stop reaction solution (2 mM EDTA). *Binding/kinetics of anti-CD63 nanobody and anti-CD63 nanobody-oligo conjugate.* His-tagged ECD-CD63 (Sino Biological) was immobilised on NTA gold sensor chip after activation of the surface with 0.5 mM Ni^{2+}. Binding affinity tests of anti-CD63 nanobody and anti-CD63 nanobody-oligo conjugate were performed by injecting increasing concentrations in single cycle kinetic mode. HBS-P+ with 50 μM EDTA buffer was flowed as running buffer over the surface. K_D, k_{on} and k_{off} were determined using the BIAevaluation 3.0 software, assuming a 1:1 binding model. *Binding/kinetics of anti-CD71 aptamer-oligo conjugate.* The biotinylated DNA oligo that is complementary to the oligo sequence used to modify the aptamer was anchored to a SA sensor chip. Aptamer-oligo conjugate was immobilised to the surface through DNA-RNA hybridization. Increasing concentrations of ECD-CD71 (Sino Biological) were injected in running buffer (HBS-EP+) over the surface in single cycle kinetic mode to determine kinetic constants (K_D, k_{on} and k_{off}).

Micropatterned surfaces presenting ECD-Her2 or ECD-Her3

Active surfaces suitable for protein immobilization were designed and fabricated by functionalization of silicon wafers with patterned Carboxymethyl-Dextran. In particular, surfaces were first coated with patterns of hydrophylic/hydrophobic surfaces by growing a Self Assembled Monolayer (SAM) of octadecyl trichloro silane (OTS) that provides the hydrophobic feature, and (3-Aminopropyl)triethoxysilane (APTES) that generates reactive regions for adhesion of Dextran. In the second step, Carboxymethyl-Dextran was deposited on the patterned reactive regions by spin coating. Carboxyl groups of dextran matrix are subsequently exploited for anchoring ECD-Her2 and ECD-Her3 through covalent amine coupling, as described above for SPR surfaces.

Cell culture and cell samples preparation

Human cancer cell lines SKBR3 and MCF7 (American Type Culture Collection; cell lines were authenticated and tested negative for mycoplasma contamination by the manufacturer) were cultured in 5% CO_2 at 37 °C in DMEM (Gibco) supplemented with 10% fetal bovine serum (Thermofisher Scientific) and 1% penicillin–streptomycin (Thermofisher Scientific). SH-SY5Y cell line (American Type Culture Collection) was cultured in 5% CO_2 at 37 °C in RPMI (Gibco) supplemented with 10% fetal bovine serum and 1% penicillin–streptomycin. To perform the NanoDeep protocol, cells were plated on 35 mm-diameter culture dishes and allowed to adhere for 24 h. Then cells were fixed with 4% formaldehyde for 20 min and washed with PBS. For ligand treatment assays, SKBR3 cells were starved for 24 h in serum-free medium and then stimulated for 15 min with 7-15 nM HRG-β1 (Sigma Aldrich).

NanoDeep on cells

Fixed SKBR3 and MCF7 cells (400,000 cells/sample), were incubated for 40 min at RT with blocking buffer (50 mM Tris-HCl pH 7.5, 150 mM NaCl, 5 mM EDTA, 250 μg/mL BSA, 15 μg/mL salmon sperm DNA (Invitrogen)) to prevent non-specific binding (Fig. S5). Three times washing with PBS + 0.05% Tween20 was then performed and, after that, Her2-NanoCombs, Her3-NanoCombs or CD71-NanoCombs were diluted in PBS + BSA 3% and incubated for 2 h at RT, followed by washing. Affibody-oligo conjugate libraries, previously hybridised with blocking strand, were next diluted in PBS + BSA 3% and added over the cells, followed by washing. Cells were then incubated at 45 °C and, after reaching the temperature, the displacement of blocking strand was performed by addition of invading strand (1 h), followed by washing. After that, cells were left at RT for 3 h to allow hybridization of binder oligos to the detection prongs. Enzymatic reactions by T4 polymerase, EcoRI and BamHI were performed as previously described. Finally, the digestion products of BamHI were recovered and supplemented with 2 mM EDTA to stop the reaction, and then concentrated by means of 3 kDa MWCO 0.5 mL Amicon centrifugal filters.

Chemiluminescence assay

Micropatterned surfaces presenting ECD-Her2 or ECD-Her3 were treated with Her2- or Her3-Nanocombs modified with desthiobiotin at the 3' end of the backbone for 2 h at RT, followed by washing. Micropatterned surfaces were then incubated with Streptavidin conjugated with HorseRadish Peroxidase (HRP) (Thermofisher Scientific) for 20 min at RT, followed by washing. 150 μL of SuperSignal™ ELISA Pico Chemiluminescent Substrate (Thermofisher Scientific) was added and substrate conversion catalysed by HRP was performed for 1 min at RT. Luminescence at 425 nm was measured within 5 min after the end of reaction with Varioskan Lux Plate Reader (Thermofisher Scientific). For the chemiluminescence assay on cells, SKBR3, MCF7 or SH-SY5Y cells, plated in 96-well white plates (Corning) were treated with Her2-NanoCombs and the chemiluminescence assay was performed as for micropatterned surfaces.

PCR amplification

GoTaq Hot start polymerase (Promega) was used for amplification of barcoded sequences derived from NanoDeep experiments. PCR was performed with the following conditions: 95 °C for 2 min, 30 cycles of 94 °C for 30 s, 38 °C for 30 s and 72 °C for 3 s, and then 72 °C for 5 min. M13F sequence (GTTTTCCCAGTCACGAC) was added at 5' of 17-nt primers to reduce non-specific PCR products. To visualise PCR products in solution, 10 μL of PCR reactions were incubated with 10 μL of SybrSafe (Thermofisher Scientific) for 20 min at RT.

NGS sequencing

Sequencing libraries were prepared using the ThruPLEX Tag-seq Kit (Takara Bio). 10 μL of samples from NanoDeep assays (performed on SPR surfaces or cells) were processed by the three-steps workflow described in the kit protocol. Reaction products were purified with Ampure-XP beads (Beckman Coulter) as follows: 0.9x volume of beads were added to 50 μL of samples and incubated for 10 min. Beads were collected with a magnet and the supernatant was transferred to different tubes and incubated with 1.8x volume of new beads for 10 min. After washing with 80% EtOH (30 s, two times), DNA was eluted with 20 μL of EB buffer (Qiagen).

Sequencing was performed using the NextSeq 550 instrument (Illumina), following the manufacturer's standard protocol. The samples were single-end sequenced with a read length of 75 bp and 8 bp index reads.

NGS Sequencing Data Analysis

The resulting sequences were analysed through cataloguing molecules by UMI's and identifying experimental barcodes using custom code written in Python and utilizing functions from the Numpy and Biopython libraries. Sequences were first processed to identify and catalog each read by its UMI according to the Tagseq pipeline. Sequences were then analysed for presence of barcode concatenation by searching by pairwise alignment (Smith-Waterman) for a common sequence and its reverse complement sequence which would be flanked by two 6-nt barcode sequences from the set of known protein identities and associated positions in the event of a concatenation. A threshold score of 80% match with the common sequence was used to select candidates for barcodes identification. Subsequent candidates were further filtered according to whether an 80% match with one of the known barcodes could be found in the 6 nucleotide positions immediately 5'

upstream and 3' downstream of the common sequence. Incidence was then tallied for each pair of barcodes identified and compiled into association matrices. Each tally was weighted by dividing its value by the UMI incidence for that particular read in order to eliminate amplification bias among associations.

Statistical analysis

Statistical analysis was carried out with GraphPad Prism (Version 8.2.1). Statistical significance was determined by performing two-tailed Student's *t*-test. A p-value ≤ 0.05 was considered statistically significant.

References

1. Orlova, A. et al. Tumor imaging using a picomolar affinity HER2 binding affibody molecule. *Cancer Res* **66**, 4339-4348 (2006).
2. Malm, M. et al. Inhibiting HER3-mediated tumor cell growth with affibody molecules engineered to low picomolar affinity by position-directed error-prone PCR-like diversification. *PLoS One* **8**, e62791 (2013).
3. Andersson, K.G. et al. Feasibility of imaging of epidermal growth factor receptor expression with ZEGFR:2377 affibody molecule labeled with 99mTc using a peptide-based cysteine-containing chelator. *Int J Oncol* **49**, 2285-2293 (2016).
4. Bernardinelli, G. & Högberg, B. Entirely enzymatic nanofabrication of DNA-protein conjugates. *Nucleic Acids Res.* **45**, e160 (2017)
5. Popovic, M., Mazzega, E., Toffoletto, B. & de Marco, A. Isolation of anti-extra-cellular vesicle single-domain antibodies by direct panning on vesicle-enriched fractions. *Microb Cell Fact* **17**, 6 (2018).
6. Oloketuyi, S. et al. Electrochemical immunosensor functionalized with nanobodies for the detection of the toxic microalgae Alexandrium minutum using glassy carbon electrode modified with gold nanoparticles. *Biosens Bioelectron* **154**, 112052 (2020).
7. Reddington, S.C. & Howarth, M. Secrets of a covalent interaction for biomaterials and biotechnology: SpyTag and SpyCatcher. *Curr Opin Chem Biol* **29**, 94-99 (2015).
8. Keeble, A.H. et al. Evolving Accelerated Amidation by SpyTag/SpyCatcher to Analyze Membrane Dynamics. *Angew Chem Int Ed Engl* **56**, 16521-16525 (2017).
9. Li, L., Fierer, J.O., Rapoport, T.A. & Howarth, M. Structural analysis and optimization of the covalent association between SpyCatcher and a peptide Tag. *J Mol Biol* **426**, 309-317 (2014).
10. Zakeri, B. et al. Peptide tag forming a rapid covalent bond to a protein, through engineering a bacterial adhesin. *Proc Natl Acad Sci U S A* **109**, E690-697 (2012).
11. Hatlem, D., Trunk, T., Linke, D. & Leo, J.C. Catching a SPY: Using the SpyCatcher-SpyTag and Related Systems for Labeling and Localizing Bacterial Proteins. *Int J Mol Sci* **20** (2019).